Hindawi
Journal of GeoEnergy
Volume 2023, Article ID 6106360, 16 pages
https://doi.org/10.1155/2023/6106360

Research Article

Technical Performance Comparison of Horizontal and Vertical Ground-Source Heat Pump Systems

Wu Gao,[1] **Shakil Masum**,[1] **and Liangliang Jiang**[2]

[1]*School of Engineering, Cardiff University, The Queen's Building, The Parade, Cardiff CF24 3AA, UK*
[2]*Department of Chemical and Petroleum Engineering, The University of Calgary, Calgary, Alberta, Canada*

Correspondence should be addressed to Wu Gao; gaowu_ed@163.com

Received 2 April 2023; Revised 31 July 2023; Accepted 23 August 2023; Published 23 September 2023

Academic Editor: Anqi Shen

The configurations of ground heat exchangers (GHEs) play a significant role in the efficiency and sustainability of ground-source heat pump (GSHP) systems. However, there is a knowledge gap in understanding the performance differences between the horizontal and vertical GSHP systems in the same project under various heating and cooling demands. In this study, a technical performance comparison between GSHP systems coupled with horizontal ground loops and vertical boreholes under three scenarios of heating-to-cooling ratios (6 : 1, 2.4 : 1, and 1 : 1) was conducted. The simulations were based on a coupled thermal–hydraulic model for unsaturated soils that takes into account realistic ground surface boundary, GHE boundary, and the dynamics of heat pump efficiency. The GHEs were designed based on an experimental site located on the campus of a UK university. Results showed significant differences in the development of fluid temperatures and coefficient of performance (COP) of heat pumps between the horizontal and vertical GSHP systems due to the differences in the soil profiles and temperature boundaries. Both the fluid temperatures and heat pump COPs in the horizontal GSHP system reached a steady annual cycle after 2 years regardless of the heating-to-cooling ratios. For the vertical system, a general downward trend in the fluid temperatures and the COP of the heat pump in the heating mode can be found when a heating-to-cooling ratio was 6 : 1 or 2.4 : 1, while an overall upward trend in the fluid temperatures and the COP of the heat pump in the heating mode can be noted in the case of 1 : 1 heating-to-cooling ratio. Additionally, the heat pump operating in the cooling mode was off most of the time when a heating-to-cooling ratio was 6 : 1 or 2.4 : 1, while a declining trend in the COP of the heat pump in the cooling mode was exhibited in the case of a heating-to-cooling ratio of 1 : 1. The technical comparison reveals that the heating-to-cooling ratios would significantly affect the efficiency and sustainability of both GSHP systems.

1. Introduction

Climate change is an urgent global concern due to the large amount of greenhouse gases (GHG) emitted into the atmosphere [1]. Fossil fuel consumption in sectors such as transport, business, and residential is largely responsible for the GHG emission. In the UK, for instance, it is reported that the residential sector emitted 68.1 $MtCO_2$, accounting for 19.9% of all carbon dioxide emissions in 2021, and the main source is the use of natural gas to heat homes [2]. With the increasing awareness of environmental protection and energy sustainability and security, shallow ground-source heat becomes a promising alternative to conventional fossil fuels to reduce the GHG emission for heating and cooling applications in residential, commercial, and public buildings [3–7].

Ground-source heat pump (GSHP) systems are usually installed to utilize the shallow ground-source heat [8, 9]. Depending on the configuration of ground heat exchangers (GHEs), GSHP systems can be classified as open or closed-loop systems. Closed-loop GSHP systems can be further divided into two types based on the installation orientation of the GHEs [10]. One is the GSHP system coupled with vertical boreholes, which usually reach depths of 15–200 m [11, 12]. The other is the GSHP system coupled with horizontal ground loops, which are installed in trenches at a depth of 1–3 m [10, 13]. These two types of GSHP systems are referred to as vertical and horizontal GSHP systems, respectively, in this study.

Numerical and experimental studies were conducted to investigate the technical and economic performance of horizontal GSHP systems under the various influential factors, including design configurations and climatic conditions. For example, Li et al. [10] developed a numerical model, which considered the geothermal gradient and varying ambient air temperature, to investigate the operating characteristics of horizontal spiral-coil GSHP system under the influences of soil thermal conductivity, buried depth, pipe spacing, and ambient air temperature. The study indicated that the soil thermal conductivity and pipe spacing are the main influential factors. Sedaghat et al. [14] proposed a ground thermal recovery system for horizontal GHEs in a hot climate, which supplied ambient-temperature air to the ground-air pipes installed between the GHEs to remove the accumulated heat from the ground. The effects of GHE length, pipe spacing, buried depth, and ground-air pipe diameter on the system performance were numerically studied and it was found that the annual coefficient of performance (COP) of the system was increased. Gao et al. [15] carried out a sandy soil container experiment to compare the thermal performance of a horizontal GHE with and without the supply of rainwater. The experiment showed the performance improvement of the system by rainwater harvest due to the increased thermal conductivity by increased moisture content. Kayaci and Demir [16] conduct an experiment to investigate the transient soil temperature profile (the horizontal and vertical temperature distribution in soil) of a horizontal GSHP system under the influences of real climatic conditions, and economic analyses considering the initial investment and operational costs were employed to study the effects of the increase rate in electricity prices, number of pipes, burial depth, pipe spacing, pipe diameter, and pipe length on the system.

The performance of vertical GSHP systems was also investigated numerically and experimentally. For example, Hein et al. [17] developed a numerical model, which included the groundwater flow and heat transport processes and the dynamics of heat pump efficiency, to study the sustainability and efficiency of vertical GSHP systems. It was found that groundwater flow and injection of excess heat would be beneficial to the energy recovery and efficiency of the heat pump. Li et al. [18] constructed a numerical model to analyse the influence of unsaturated soil properties and groundwater flow on the performance of vertical GSHP systems. The simulated results showed that neglecting variations in moisture content in unsaturated soil would underestimate the heat transfer capacity of the soil, and a rising groundwater table was beneficial to the heat transfer of the borehole and the operation of the vertical GSHP system. In addition, Soltani et al. [19] numerically investigated the capacity of various circulating fluids and their effects on energy consumption reduction of vertical GSHP systems. The simulations showed that utilizing varying levels of ethylene glycol, methanol, potassium acetate, sodium chloride, and Freezium as the heat carrier fluid would decrease the energy consumption significantly compared to the pure water. Boughanmi et al. [20] experimentally examine the performance of a vertical GSHP system coupled with a conic basket pipe for greenhouse cooling. Monitored results indicated that the air temperature inside the greenhouse decreased by 8–12°C with the operation of the cooling system.

Except for the individual study on the horizontal or vertical GSHP systems, research studies also compared the performance between the horizontal and vertical GSHP systems. To demonstrate the technical and design feasibility of GSHP systems in mild climate applications for greenhouse heating, Benli [21] conducted an experimental comparison using a heating system consisting of two different GHEs. Results showed that the heating COP of the overall system was 2.7–3.3 for the horizontal system and 2.9–3.5 for the vertical system. Lee et al. [22] carried out a field test to analyse the performance of GSHP systems when the coil-type GHE was installed horizontally or vertically. It was found that the amount of electric power consumed by the horizontal system was higher than that consumed by the vertical system, and the cooling COP was 3.9–4.3 for the vertical system and 3.3–3.7 for the horizontal system. Yin et al. [23] compared the field performance of GSHP systems for residential space heating based on 32 residential houses with 16 vertical and 16 horizontal GHEs. Results showed the COP for horizontal systems ranged from 1.18 to 4.57 while the COP for vertical systems demonstrated less variation (1.96–3.8) due to more stable ground temperatures given the fact that vertical GHEs reached deeper into the ground than the horizontal GHEs. Furthermore, on the basis of a case study of a residential building with a fixed heating and cooling load under moderate climate conditions, Aresti et al. [24] performed a life cycle analysis (LCA) for a direct environmental impact comparison between different GHE configurations, including three types vertical GHEs and five types horizontal GHEs. It was found that the vertical coaxial GHE configuration led to the most negative environmental impact among all GHE configurations, and the horizontal GHEs outperformed the vertical GHEs in all impact categories.

Based on the literature review conducted, it becomes evident that the configuration of the GHEs is pivotal in determining the efficiency and sustainability of GSHP systems. However, a notable knowledge gap exists regarding the performance disparities between horizontal and vertical GSHP systems within the same project, particularly when confronted with varying heating and cooling demands. This knowledge gap consequently hinders the selection of appropriate GHEs to ensure the optimal performance of GSHP systems.

To address this research gap, this study focuses on a technical performance comparison between a horizontal GSHP system and a vertical GSHP system under the three distinct scenarios characterised by varying heating-to-cooling ratios. To conduct these comparisons, a coupled thermal–hydraulic (TH) model for unsaturated soils has been employed, which takes into account realistic ground surface boundaries, GHE boundary, and the dynamics of heat pump efficiency. Furthermore, the design of the GHEs utilised information gathered from an experimental site situated on the campus of a UK university.

This paper is structured as follows: first, a comprehensive description of the numerical model employed in this study is presented. After that, the model validation is provided. Next, the model is applied to the experimental site, and subsequently, results derived from the simulations and discussion are given. Finally, conclusions are drawn.

2. Numerical Model

2.1. Moisture and Heat Transfer in Unsaturated Soils. Shallow ground is generally unsaturated. The governing equation of moisture transfer within unsaturated soils can be given as follows [25]:

$$\rho_l \frac{\partial \theta_l}{\partial t} + \frac{\partial (\rho_v \theta_a)}{\partial t} = -\rho_l \nabla \cdot v_l - \rho_l \nabla \cdot v_v. \tag{1}$$

As shown in Equation (1), moisture in unsaturated soils consists of liquid water and vapour.θ_l is the volumetric water content (-), θ_a is the volumetric air content (-), t is the time (s), ∇ is the gradient operator, ρ_l is the density of the water (kg/m^3), ρ_v is the density of vapour (kg/m^3), v_l is the velocity of water (m/s), and v_v is the velocity of vapour (m/s).

Using Darcy's law and the equation proposed by Philip and Vries [26], the velocities of water and vapour are obtained, respectively:

$$v_l = -K_l \left(\nabla \frac{u_l}{\gamma_l} + \nabla y \right), \tag{2}$$

$$v_v = -\frac{D_{\text{atms}} v_v \tau_v \theta_a}{\rho_l} \nabla \rho_v, \tag{3}$$

where u_l is the pore-water pressure (Pa), γ_l is the unit weight of water (N/m^3), y is the elevation (m), D_{atms} is the molecular diffusivity of vapour through air, and $D_{\text{atms}} = 5.893 \times 10^{-6} T^{2.3}/u_a$ with $u_a = 1\text{atm}$, v_v is a mass flow factor (-), τ_v is a tortuosity factor (-), and $\nabla \rho_v$ is the spatial vapour density gradient.

K_l in Equation (2) is the unsaturated hydraulic conductivity, expressed by the Brooks and Corey [27] Model:

$$K_l = K_{ls} \left(\frac{\theta_l}{\theta_{ls}} \right)^{\eta}, \tag{4}$$

in which K_{ls} is the saturated hydraulic conductivity (m/s), θ_{ls} is the saturated water content (-), and η is the shape parameter (-).

The van Genuchten [28] model is used to characterize the soil water characteristic curve of soils:

$$\frac{\theta_l}{\theta_{ls}} = \left[1 + \left(\frac{h}{h_d} \right)^n \right]^{\left(\frac{2}{n} - 1\right)}, \tag{5}$$

where h is the pressure head (m), h_d is the scale parameter (m), and n is the shape parameter (-).

The volumetric energy balance within unsaturated soils can be expressed [25]:

$$\frac{\partial [H_c (T - T_r) + L \varphi S_a \rho_v]}{\partial t} = -\nabla \cdot [-\lambda_T \nabla T + L(v_v \rho_l) + (C_{pl} v_l \rho_l + C_{pv} v_v \rho_l)(T - T_r)], \tag{6}$$

where T is the temperature (K), L is the latent heat of vaporisation (J/kg), ϕ is the soil porosity (-), S_a is the saturation degree of pore air (-), and H_c is the unsaturated soil's heat capacity at a reference temperature T_r, in J/m^3/K, C_{pl} and C_{pv} are the specific heat capacities of water and vapour, respectively, in J/kg/K, and λ_T is the thermal conductivity for the unsaturated soil (W/m/K).

The heat capacity of the unsaturated soil can be obtained as below:

$$H_c = (1 - \phi) C_{ps} \rho_s + \phi (C_{pl} S_l \rho_l + C_{pv} S_a \rho_v), \tag{7}$$

where C_{ps} is the specific heat capacities of the solid (J/kg/K), S_l is the degree of saturation of water (-), and ρ_s is the density of the solid (kg/m^3).

Moreover, the thermal conductivity for the unsaturated soil can be obtained based on the soil's components as follows [29]:

$$\lambda_T = \lambda_s^{\chi_s} \cdot \lambda_w^{\chi_w} \cdot \lambda_a^{\chi_a}, \tag{8}$$

where λ_s, λ_w, and λ_a is the thermal conductivity corresponding to the solid, water, and air, respectively, in W/m/K, and χ_s, χ_w, and χ_a is the volume fraction corresponding to the solid, water, and air, respectively, which can be calculated by the following equations:

$$\begin{aligned} \chi_s &= 1 - \phi, \\ \chi_w &= \phi S_l, \\ \chi_a &= \phi (1 - S_l). \end{aligned} \tag{9}$$

2.2. Boundaries for GSHP Systems

2.2.1. Ground Surface Boundary. For a GSHP system coupled with horizontal ground loops, its performance is significantly affected by the heat and moisture exchanges at the ground surface [30]. The energy balance equation at the ground surface is as follows [6]:

$$F_{\text{NE}} = F_{\text{SW}}^{\text{absorbed}} + \left(F_{\text{LW}}^{\text{absorbed}} - F_{\text{LW}}^{\text{emitted}} \right) - F_{\text{SEN}} - F_{\text{LE}}, \tag{10}$$

where F_{NE} is the net radiant energy flux absorbed or emitted at the ground surface (W/m^2), $F_{\text{SW}}^{\text{absorbed}}$ is the absorbed shortwave radiation flux (W/m^2), $F_{\text{LW}}^{\text{absorbed}}$ is the absorbed longwave radiation flux (W/m^2), $F_{\text{LW}}^{\text{emitted}}$ is the emitted longwave radiation flux (W/m^2), F_{SEN} is the sensible heat flux (W/m^2), and F_{LE} is the latent heat flux (W/m^2). The sensible heat flux is the transfer of heat caused by the difference in temperature between the ground surface and the air. The latent heat flux is the heat moved by the water evaporation.

The moisture balance at the ground surface is presented below [31]:

$$M_{\mathrm{NM}} = P - E_{\mathrm{AE}} - R_{\mathrm{RO}}, \tag{11}$$

in which M_{NM} is the net moisture flux at the ground surface (kg/m^2/s), P is the rainfall (kg/m^2/s), E_{AE} is the actual evaporation flux (kg/m^2/s) and R_{RO} is the run-off (kg/m^2/s). The expression of each term in Equations (10) and (11) are detailed in [30].

Five climatic variables are needed to determine the ground surface boundary in terms of energy and moisture transfer of the coupled TH model, and they are ambient air temperature, shortwave solar radiation, air relative humidity, wind speed, and rainfall.

2.2.2. Ground Heat Exchanger Boundary. With the circulation of fluid in the GHE, there is the following relationship between inlet fluid temperature and outlet fluid temperature:

$$T_{f,i} = T_{f,o} - \frac{Q_{\mathrm{GHE}}}{C_{pf} \cdot \rho_f \cdot r_f}, \tag{12}$$

where $T_{f,i}$ is the inlet fluid temperature (K), $T_{f,o}$ is the outlet fluid temperature (K), C_{pf} is the specific heat capacity of the fluid (J/kg/K), ρ_f is the fluid density (kg/m^3), and r_f is the fluid flow rate (m^3/s), and Q_{GHE} is the thermal load of the GHE, in W (positive in heating mode, negative in cooling mode).

The GHE in the model is discretized into a series of control volumes with a length of dL, and the fluid temperature in each control volume $T_{f,j}$ is assumed to be constant. The heat flux at the GHE boundary F_{GHE} can be obtained based on Fourier's law:

$$F_{\mathrm{GHE}} = \frac{T_g - T_{f,j}}{R_{\mathrm{res}} \cdot 2\pi \cdot R \cdot dL}, \tag{13}$$

where T_g is the ground temperature adjacent to the control volume j in K, and R is the outer radius of pipes (m), and R_{res} is the thermal resistance of pipes (K/m), which can be calculated as follows:

$$R_{\mathrm{res}} = \frac{\ln[R/(R-b)]}{2\pi \cdot dL \cdot \lambda_p}, \tag{14}$$

where b is the thickness of pipes (m) and λ_p is the thermal conductivity of pipes (W/m/K).

2.3. COP of Heat Pump. The thermal load of the GHE in the heating and cooling modes, respectively, can be calculated based on the building thermal load Q_{building} (W) and the heat pump's COP (-) as follows:

$$\begin{aligned} Q_{\mathrm{GHE}}^{\mathrm{heating}} &= Q_{\mathrm{building}}\left(1 - \frac{1}{\mathrm{COP}_{\mathrm{heating}}}\right), \\ Q_{\mathrm{GHE}}^{\mathrm{cooling}} &= Q_{\mathrm{building}}\left(1 + \frac{1}{\mathrm{COP}_{\mathrm{cooling}}}\right), \end{aligned} \tag{15}$$

The empirical model proposed by Staffell et al. [32] is employed to predict the COP of a heat pump. The model was obtained by fitting the temperature difference and the heat pump COP data taken from industrial surveys and field trials:

$$\begin{aligned} \mathrm{COP}_{\mathrm{heating}} &= 8.77 - 0.15\Delta T + 0.000734\Delta T^2, \\ \mathrm{COP}_{\mathrm{cooling}} &= \mathrm{COP}_{\mathrm{heating}} - 1, \\ \Delta T &= \begin{cases} \left|T_{\mathrm{hot}} - T_{f,o}\right| \text{heating mode} \\ \left|T_{f,o} - T_{\mathrm{chilled}}\right| \text{cooling mode} \end{cases}, \end{aligned} \tag{16}$$

where ΔT is the temperature difference (K), T_{hot} is the temperature of the supplied hot water to the building (K), and T_{chilled} is the temperature of the supplied chilled water to the building (K). In this study, the values of T_{hot} and T_{chilled} are set as 315.65 and 282.65 K, respectively (namely 42.5°C and 9.5°C, respectively) [33]. Therefore, when the outlet fluid temperature increased above 315.65 K (42.5°C) or dropped below 282.65 K (9.5°C), respectively, the free heating or free cooling operation would be available, i.e., heat pumps would stop, and the thermal load of the GHE equalled the building thermal load.

2.4. Numerical Solutions. The proposed coupled model is implemented into a thermal–hydraulic-chemical–mechanical (THCM) modelling platform—COMPASS (code of modelling prtially saturated soils) [34]. The governing equations can be expressed in terms of pore-water pressure and temperature as follows:

$$\boldsymbol{C_{ll}}\frac{\partial u_l}{\partial t} + \boldsymbol{C_{lT}}\frac{\partial T}{\partial t} = \nabla \cdot [\boldsymbol{K_{ll}}\nabla u_l] + \nabla \cdot [\boldsymbol{K_{lT}}\nabla T] + \boldsymbol{J_l}, \tag{17}$$

$$\boldsymbol{C_{TT}}\frac{\partial T}{\partial t} + \boldsymbol{C_{Tl}}\frac{\partial u_l}{\partial t} = \nabla \cdot [\boldsymbol{K_{TT}}\nabla T] + \nabla \cdot [\boldsymbol{K_{Tl}}\nabla u_l] + \boldsymbol{J_T}, \tag{18}$$

where $\boldsymbol{C_{ll}}$, $\boldsymbol{C_{lT}}$, $\boldsymbol{C_{TT}}$, $\boldsymbol{C_{Tl}}$, $\boldsymbol{K_{ll}}$, $\boldsymbol{K_{lT}}$, $\boldsymbol{K_{TT}}$, $\boldsymbol{K_{Tl}}$, $\boldsymbol{J_l}$ and $\boldsymbol{J_T}$ are detailed by Gao et al. [25].

The Galerkin finite-element method [35] is employed to spatially discretize the governing equations of the coupled model, and an implicit mid-interval backward difference time-stepping algorithm is employed for the temporal discretisation. The discretised system of linear equations is solved iteratively using a predictor-corrector algorithm [36] to obtain the ground temperature and pore-water pressure

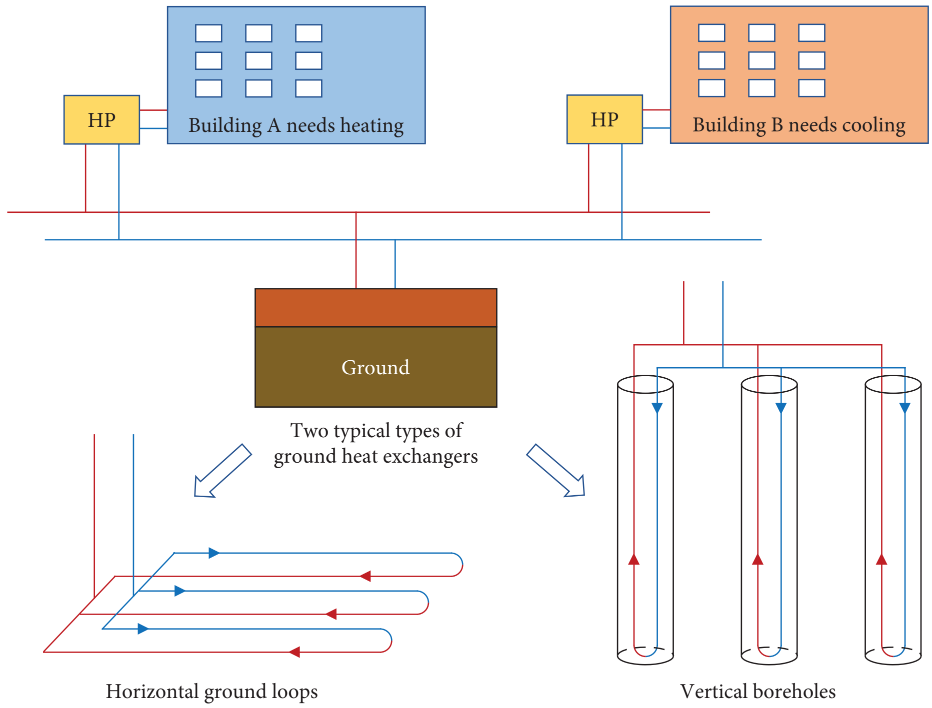

Figure 1: A schematic diagram illustrating the main components of the GSHP system (HP means heat pump).

distributions. A local time-step is prescribed between two consecutive global time-steps, and the fluid temperature profile is calculated. The fluid circulation can be modelled by repeating the multiple time-steps procedure. Meanwhile, the updated fluid temperature profile is used to update the heat flux at the GHE boundary to obtain the ground thermal behaviour.

3. Model Validation

The TH model presented in this study has been previously thoroughly validated against the experimental data, including an evaporation monitoring study in the Southern France [37, 38], an on-site heating experiment utilising a vertical borehole installed in a three-layered ground [39], and a laboratory heating experiment involving a horizontal GHE in a two-layered ground [40], as well as established numerical solution [39]. The numerical results predicted by this model showed great agreement with the experimental data and numerical results. Due to the length constraints, readers interested in further details are referred [30, 41].

4. Model Application

4.1. Experimental Site. The technical performance comparisons are conducted based on an experimental site located in a UK university [25, 30]. As shown in Figure 1, a GSHP system, which can be coupled with two typical types of GHEs, i.e., horizontal ground loops and vertical boreholes, was constructed to provide heating and cooling for campus buildings. The GHEs were designed to connect in parallel to reduce the thermal interferences between each other when heat was extracted from or injected into the ground. Two buildings (A and B), a student accommodation and a data centre, with different heat demands were each equipped with a water source heat pump and connected to the respective GSHP systems.

4.2. Thermal Load of Buildings. Figures 2(a) and 2(b) illustrate the total heating load from Building A and the total cooling load from Building B, respectively, which are provided monthly. The heating load data were collected and provided by the Estate Office of the university, and the cooling load data were estimated by the consultation and experience. It should be noted that three scenarios of total cooling load were planned, which corresponded to a heating-to-cooling ratio (H : C) of 6 : 1, 2.4 : 1, and 1 : 1, respectively, to investigate the effects of heating-to-cooling ratios on the thermal behaviour of the GSHP system. In this study, the connections between the heat pumps and the network were not modelled. The total thermal load applied to the GHEs was the sum of the regulated building thermal loads from these two buildings based on Equations (15) and (16).

4.3. D Domains

4.3.1. Horizontal Ground Loops. Based on the available land area near the two buildings, as well as to minimize the thermal interferences between the GHEs, the configurations of the GHEs in the GSHP system were designed. For the GSHP system coupled with horizontal ground loops, it was comprised of 200 U-tube ground loops buried at 3.0 m below the ground surface ($H = 3.0$ m). A representative unit of the horizontal ground loops is illustrated in Figure 3. The length (L) and the spacing (S) of each leg of the U-tube ground loops were 200.0 and 1.0 m, respectively. The outer radius (R) of

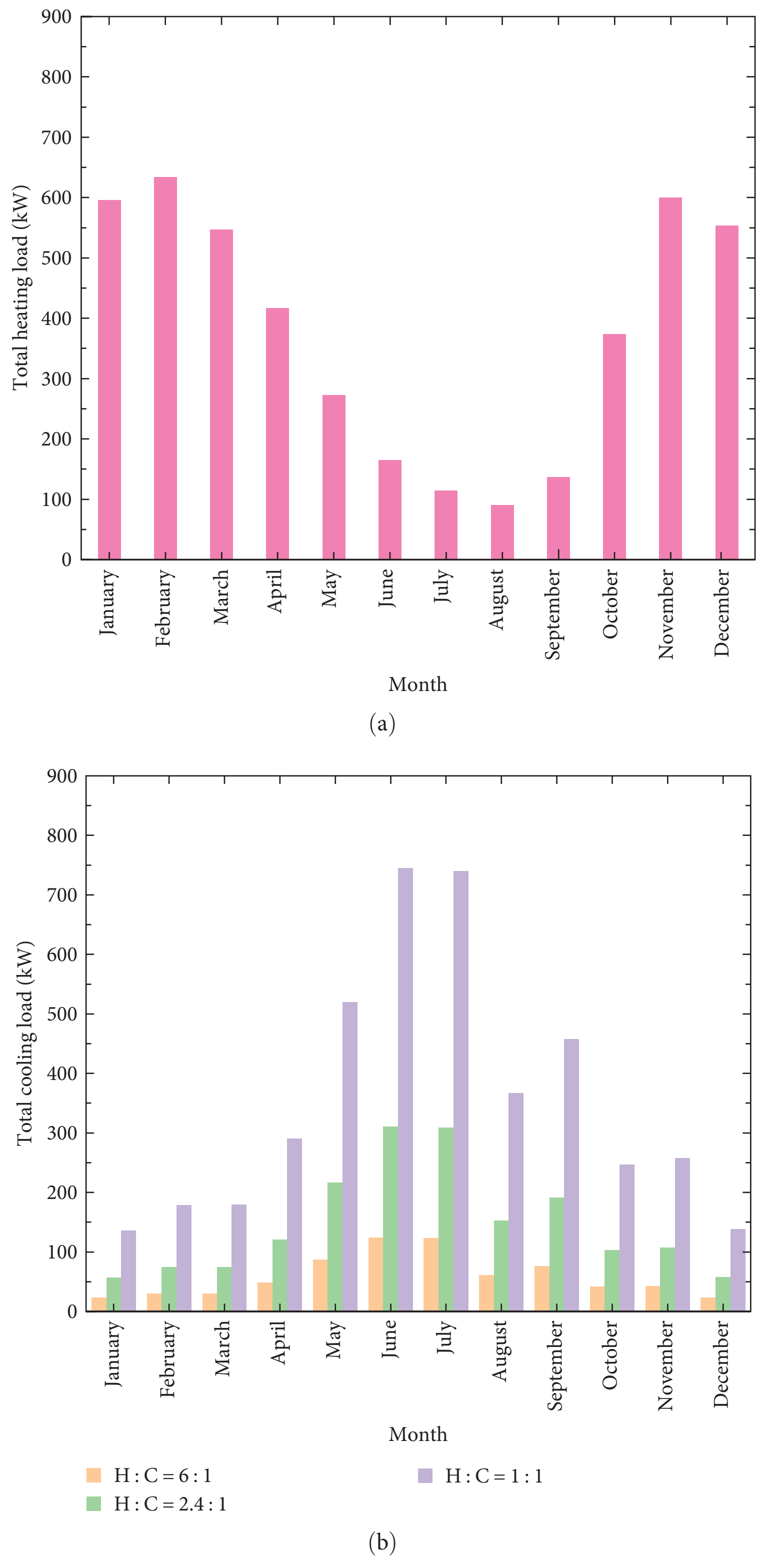

Figure 2: Thermal load of buildings: (a) heating load and (b) cooling load.

the ground loop pipes was 0.02 m and the pipe thickness (b) was 0.003 m. The thermal conductivity of pipe material (λ_p) was 0.45–W/m/K. Along the depth of the 3D domain ($D = 4.0$ m), three different soil layers were identified based on the borehole logs from the British Geological Survey [42]. The corresponding soil parameters are given in Table 1.

To enhance computational efficiency while maintaining accuracy, ground surface temperature, and pore-water pressure

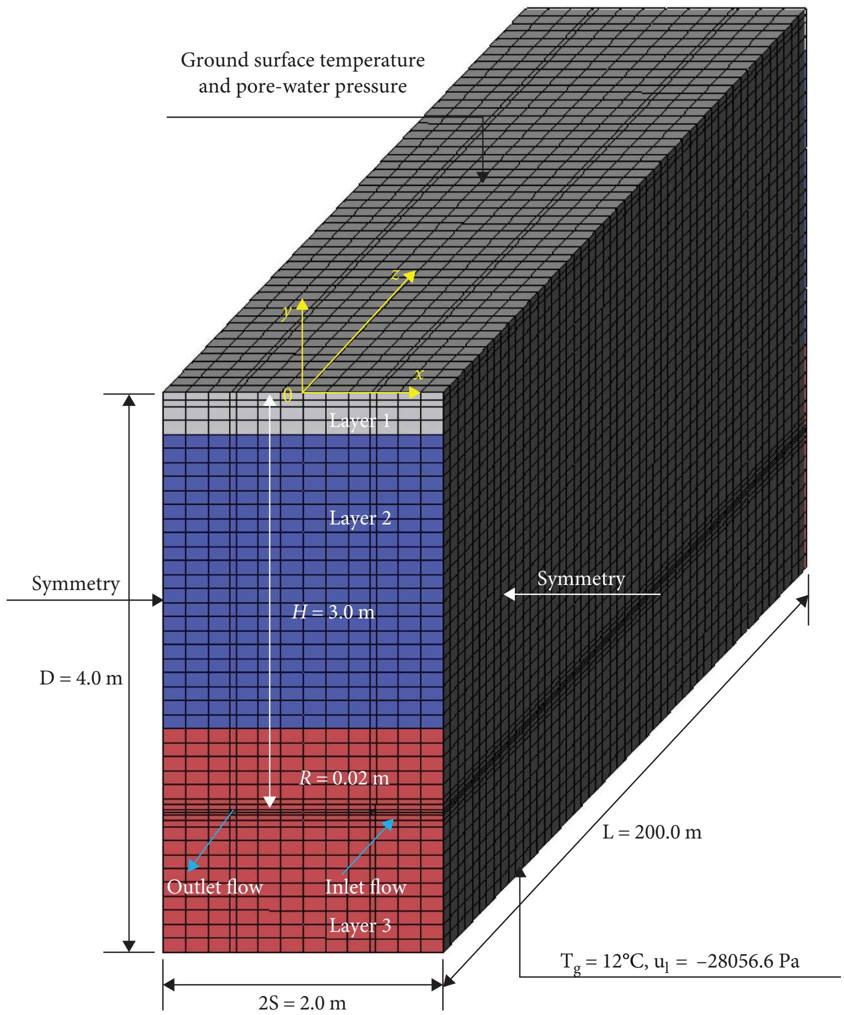

FIGURE 3: Schematic shows the initial and boundary conditions and 3D discretized mesh for a representative unit of the horizontal ground loops [25].

TABLE 1: Material parameters of three soil layers below the ground surface [25, 30].

Layer	Soil	D (m)	φ (-)	θ_{ls} (-)	h_d (m)	n (-)	K_{ls} (m/s)	η (-)	ρ_s (kg/m^3)	C_{ps} (J/kg/K)	λ_s (W/m/K)
1	Sandy clay loam	0–0.3	0.51	0.51	0.123	2.095	6.400E-7	3.67	2630.0	1014.0	1.04
2	Silty clay	0.3–2.4	0.60	0.60	0.471	2.223	4.051E-7	5.04	2800.0	1169.0	3.76
3	Mudstone	2.4–4.0	0.51	0.51	1.020	2.268	1.882E-6	17.12	2435.0	1050.6	2.42

have been prescribed at the domain surface, which were determined by the local climatic conditions in the year of 2019, including ambient air temperature, shortwave solar, air relative humidity, and wind speed [25]. It should be noted that the variations in the climatic conditions are not considered for the 5-year-long simulations in the current study. At the bottom of the domain, a fixed ground temperature (T_g) of 12.0°C was applied based on the literature [43] and a saturation of 0.75 were assumed considering the local shallow groundwater level. Pure water with an initial temperature (T_f) of 12.0°C was adopted as the heat carrier fluid, which entered from the right inlet and exited from the left outlet. A constant difference of 4°C between the outlet and inlet fluid temperatures was set. In addition, the specific heat capacity (C_{pf}) and the density (ρ_f) of pure water were taken as 4180.0 J/kg/K and 1000.0 kg/m^3, respectively.

4.3.2. Vertical Boreholes. The GSHP system coupled with 200 vertical boreholes was also designed. These vertical boreholes were evenly distributed in the experimental site with a spacing of 8.0 m between each other and were arranged in a regular hexagon layout. Figure 4 shows the 3D domain for a representative unit of the vertical boreholes. As can be seen from the figure, only half of the domain with a width (W) of 4.0 m is needed for the simulation due to the symmetry of the vertical boreholes. Similar to the horizontal ground loops,

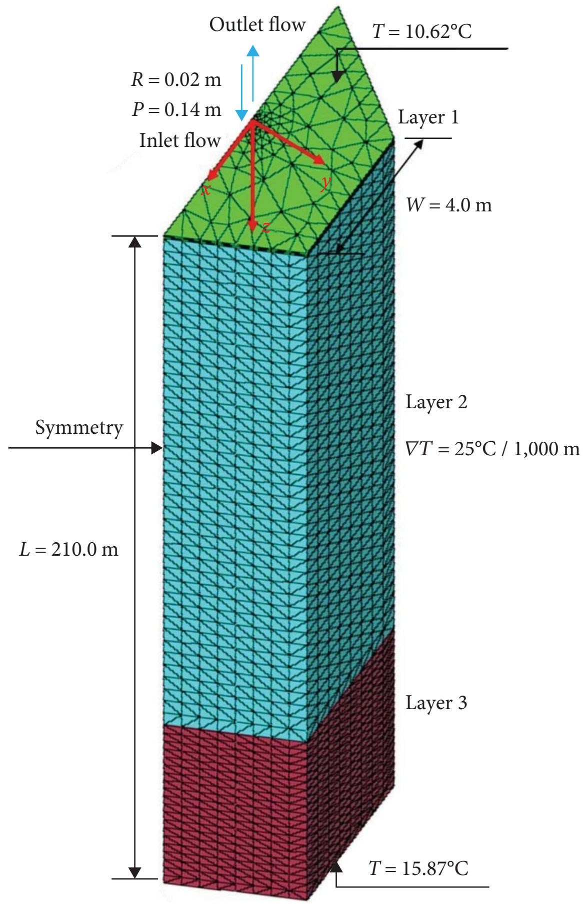

Figure 4: Schematic shows the initial and boundary conditions and 3D discretized mesh for a representative unit of the vertical boreholes.

Table 2: Parameters for geologic materials and the ground along the depth of the vertical borehole [30, 39, 45].

Layer	Material	D (m)	φ (-)	λ_s (W/m/K)	ρ_s (kg/m^3)	C_{ps} (J/kg/K)	K_{ls} (m/s)	S_l (-)
1	Silty clay	0–1.2	0.60	3.76	2800.0	1169.0	4.051E-7	1.0
2	Mudstone	1.2–158.8	0.51	2.42	2435.0	1051.0	1.882E-6	1.0
3	Sandstone	158.8–210.0	0.15	2.83	2668.0	833.0	1.74E-5	1.0
1–3	Grout	0–210.0	0.42	1.85	1847.0	1512.0	4.53E-6	1.0

the length (L) of each vertical borehole was 210.0 m. Consequently, the total length of the two types of GHEs is comparable in the two systems.

These vertical boreholes passed through three soil/rock layers, which can be considered saturated without no groundwater flow based on the local borehole logs. Table 2 gives the material parameters for geologic materials and the grout. Moreover, the same size U-tube pipe as in the horizontal ground loops was installed in each vertical borehole with a diameter (P) of 0.14 m, and the spacing between the two legs of the U-tube pipe (S) was 0.06 m. It should be pointed out that these vertical boreholes were buried 1.2 m below the ground surface to avoid the influence of varied ground surface temperature due to the local climatic conditions, therefore, a fixed temperature (T) of 10.62°C corresponding to the undisturbed average ground temperature was prescribed on the top of the domain. Owing to the depth of the vertical boreholes, a temperature gradient (∇T) of 25.0°C/1,000 m was considered based on the literature [44], and hence, a constant ground temperature of 15.87°C was determined at the bottom of the domain. Pure water also circulated through each vertical borehole. It was assumed, a constant difference of 4°C between the outlet and inlet, the same as in the horizontal ground loops, ensuring the temperature differences in the warm and cold pipes in both GSHP systems are the same.

5. Results and Discussion

5.1. Horizontal GSHP System. Simulations of the GSHP system coupled with horizontal ground loops under various heating-to-cooling ratios were conducted for 5 years, which is long enough to observe the long-term patterns. As shown in Figures 5 and 6, the results of fluid temperatures and each heat pump's COP

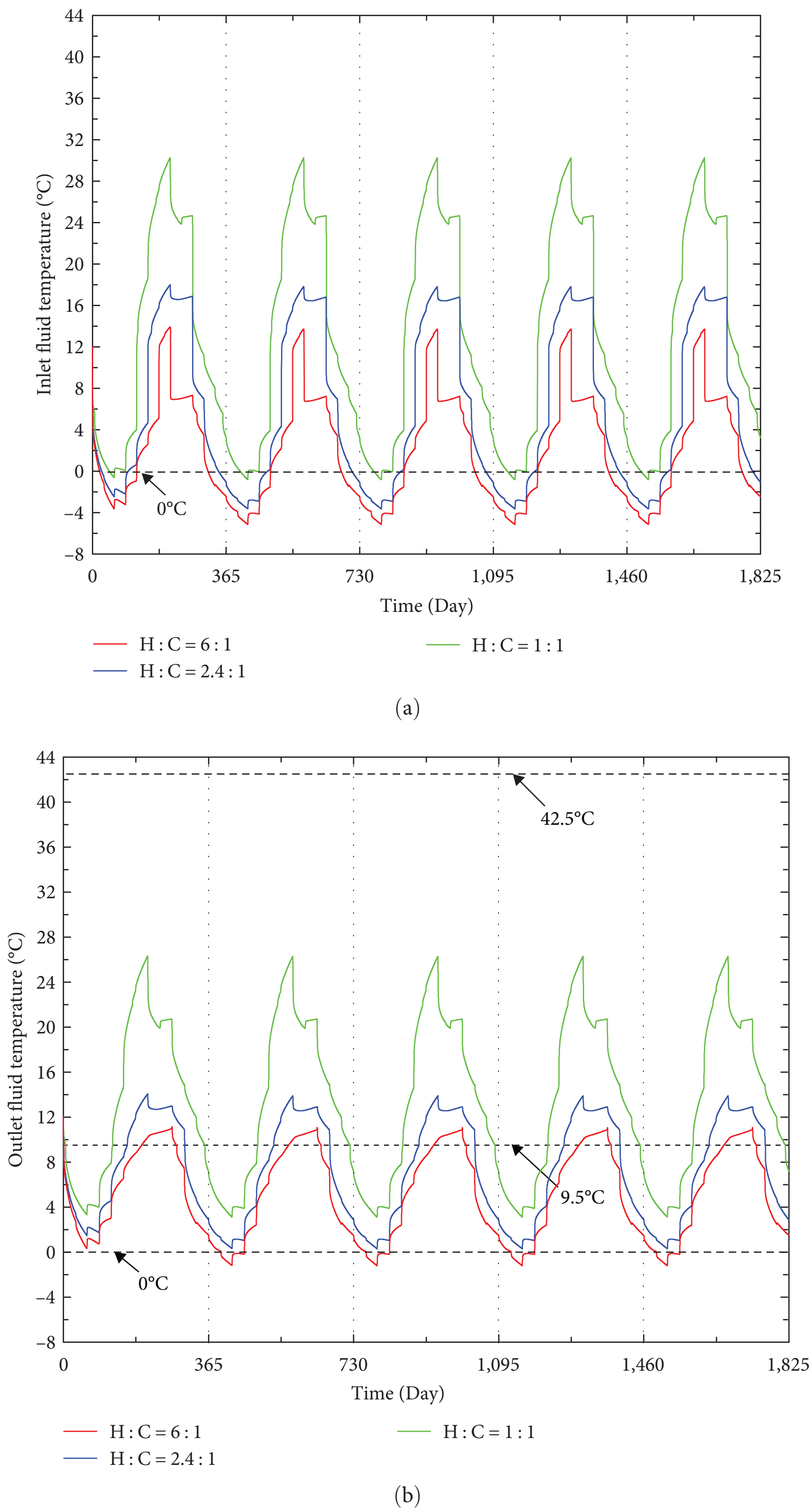

Figure 5: Variations in (a) inlet and (b) outlet fluid temperature of the horizontal GSHP system.

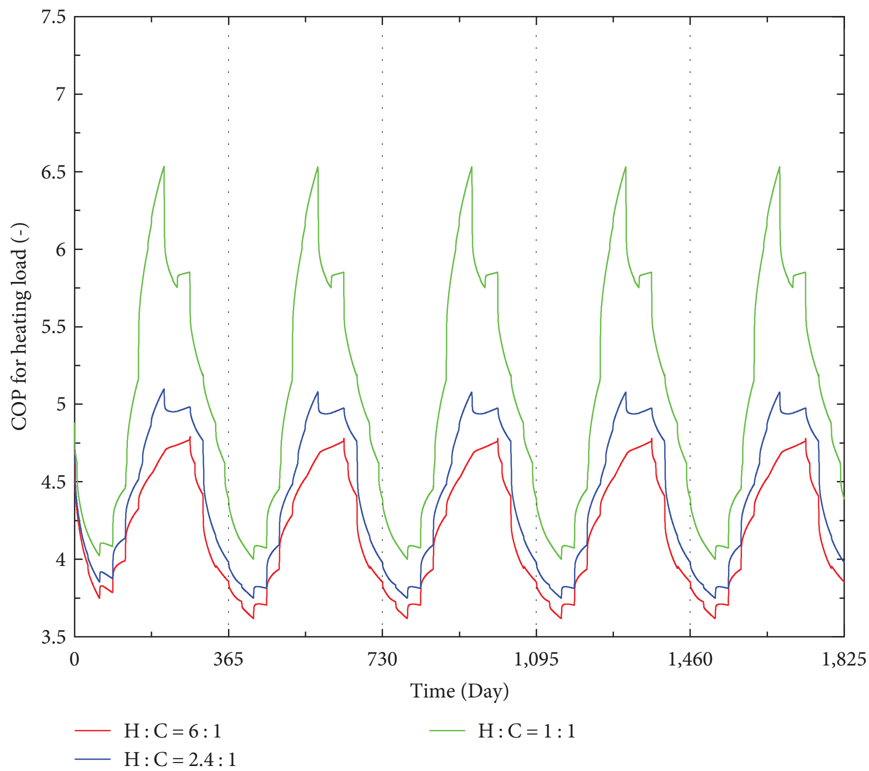

(a)

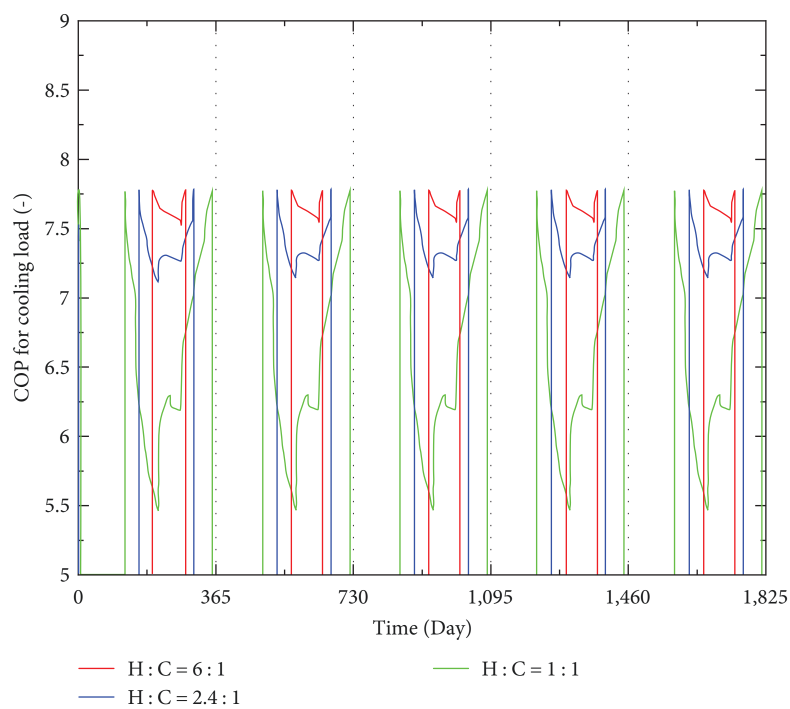

(b)

FIGURE 6: Variations in (a) COP of heat pump for heating load and (b) COP of heat pump for cooling load in the horizontal GSHP system.

during the 5-year simulation are illustrated. Upon the collective inspection of the simulated results, both the fluid temperatures and COPs of heat pumps reached a steady annual cycle after approximately 2 years regardless of the heating-to-cooling ratios. This observed cyclic behaviour was expected owing to the annually prescribed temperature and pore-water pressure on the ground surface and the fixed ground temperature and saturation at the bottom of the domain.

As demonstrated in Figure 5, the amplitude of the simulated fluid temperature increased with the decrease in the heating-to-cooling ratio, and a fixed difference of 4°C between the inlet and outlet fluid temperatures can be observed. For the scenarios of a heating-to-cooling ratio of 6 : 1 or 2.4 : 1, the inlet fluid temperature would quickly decrease below 0°C, namely the freezing point of pure water, on the 19^{th} day and 24^{th} day of the 1st year, respectively; and starting from the 2nd year, the inlet fluid temperature would always be lower than 0°C in the first 3.5 and 4 months of every year, respectively, implying the malfunction of the horizontal GSHP system. In comparison, when more heat was injected into the ground, i.e., the scenario of a heating-to-cooling ratio was 1 : 1, the lowest fluid temperature occurred at the inlet and increased to −0.83°C, and the situation when the fluid temperature was lower than 0°C would last for 20 days in February of each year. Meanwhile, since the heat would be easily dissipated in the shallow ground or fast replenished by the adjacent ground, the fluid temperature would remain dynamically stable on a yearly basis.

Figure 6 shows the COPs of two heat pumps for the heating and cooling modes, respectively. It should be noted that the heat pump's COP depends on the temperature difference between the outlet fluid temperature and the temperature of the supplied hot/chilled water to the building. The heat pump under heating mode would operate for 5 years due to the exclusion of free heating, the range of its COP varied from 3.62 and 6.53 under three heating-to-cooling ratios (Figure 6(a)). As the outlet fluid temperature was always below the temperature of the supplied hot water (42.5°C) as shown in Figure 5(b), the lower the heating-to-cooling ratios, the smaller the temperature difference, and the higher the COP under the heating mode.

In contrast, as the free cooling could happen in the three heating-to-cooling ratio scenarios (Figure 5(b)), a discontinuity in the heat pump's COP can be found in Figure 6(b). The COP for the heat pump running in cooling mode changed from 5.46 to 7.77. A higher outlet fluid temperature than the temperature of the supplied chilled water (9.5°C) would lead to a lower COP under the cooling mode. Overall, the decreasing heating-to-cooling ratios (more heat injected into the shallow ground) would improve the COP of the heat pump under heating mode, while having opposite effects on the COP of the heat pump under cooling mode.

5.2. Vertical GSHP System. Simulations of the GSHP system coupled with vertical boreholes under various heating-to-cooling ratios were carried out for 6 years to clearly exhibit the changing patterns. The results of fluid temperatures and two heat pumps' COPs under the three heating-to-cooling ratios are plotted in Figures 7 and 8, respectively.

As shown in Figure 7, a fast decline in the fluid temperatures can be observed in the 1st week of the 1st year regardless of the heating-to-cooling ratios due to the high-heating demands in January. The status of the inlet fluid temperature that was lower than 0°C would remain for 2–3 months in the 1st year in different heating-to-cooling ratio scenarios, while the fluid temperature would gradually increase above the freezing point of water mainly due to the increased cooling demand. Therefore, choosing a suitable heat carrier fluid with a low-freezing point was of importance to this system, especially to ensure its performance in the 1st year. In the long-term, a general downward trend in the fluid temperatures can be clearly noted when the heating-to-cooling ratio equalled 6 : 1 or 2.4 : 1 in the vertical system rather than a steady annual cycle as noted in the horizontal system. In comparison, when the heating-to-cooling ratio decreased to 1 : 1, i.e., more heat was injected into the ground each year through vertical boreholes, and an overall upward trend in the fluid temperature was generated.

Figures 8(a) and 8(b) illustrate the COP of the heat pump in heating mode and cooling mode, respectively. For the heat pump operating in the heating mode (Figure 8(a)), when the heating-to-cooling ratio was 6 : 1 or 2.4 : 1, the COP decreased year by year owing to the increasing difference between the outlet fluid temperature and the supplied hot water temperature (42.5°C), as shown in Figure 7(b). For example, the highest COP for the case of a heating-to-cooling ratio of 6 : 1 was 4.88 in the 1st year but decreased to 3.71 in the 6th year. In contrast with that, the COP for the case of a heating-to-cooling ratio of 1 : 1 increased year by year, for instance, the lowest COP was 3.71 in the 1st year but rose to 4.69 in the 6th year.

As shown in Figure 7(b), the situation that the outlet fluid temperature was lower than the supplied chilled water temperature (9.5°C) can be observed in all scenarios, indicating the occurrence of free cooling and the discontinuity in the heat pump's COP (Figure 8(b)). In the cases when the heating-to-cooling ratio was 6 : 1 or 2.4 : 1, the duration when the outlet fluid temperature was higher than 9.5°C lasted for a few months. Hence, in these two cases (6 : 1 and 2.4 : 1) the heat pump operating in cooling mode was off most of the time, and a high COP (>7.25) was achieved when the heat pump was running. In contrast, in the heating-to-cooling ratio of 1 : 1 scenario, the increasing temperature difference between the outlet fluid and the supplied chilled water on one hand increases the cooling operational period of the heat pump annually, on the other hand, led to a general downward trend in COP in cooling mode.

5.3. Comparisons between the Horizontal and Vertical Systems. Table 3 compares GSHP systems coupled with horizontal ground loops and vertical boreholes from a technical point of view. As can be seen from the table, the land area of horizontal ground loops was approximately 9.6 times the floor area of the vertical boreholes. Owing to the differences in the soil profiles and temperature boundaries as listed in the table, the fluid temperatures and two heat pumps' COPs under three heating-to-cooling ratios exhibited disparate trends and results.

As shown in Figure 5, an annual periodic pattern in the fluid temperatures and heat pump's COPs regardless of the heating-to-cooling ratios indicated a high-natural heat regeneration potential yet unideal heat storage capacity for the horizontal system. As shown in Figure 7, for the vertical system, a downward trend in the fluid temperatures when the

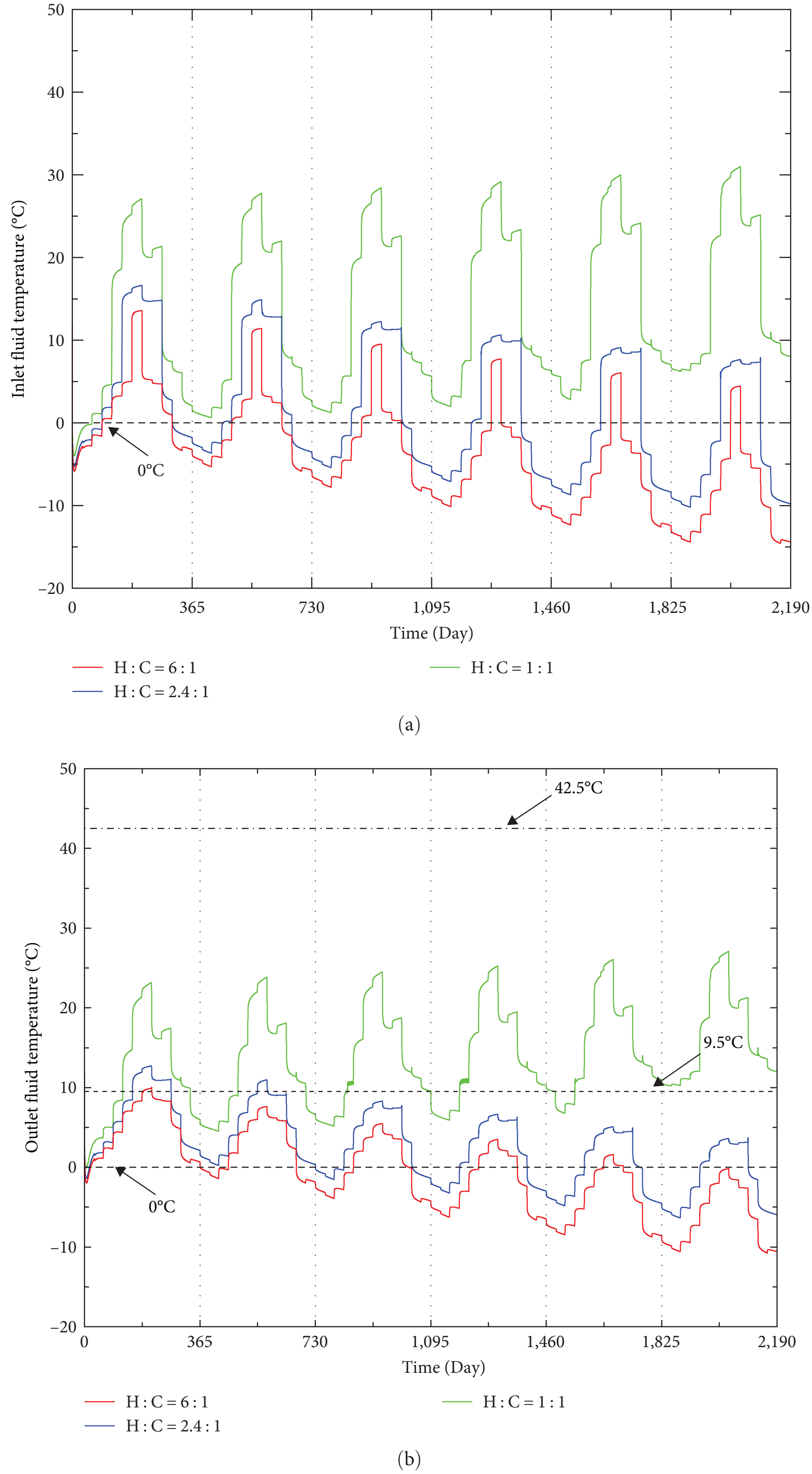

Figure 7: Variations in (a) inlet and (b) outlet fluid temperature of the vertical GSHP system.

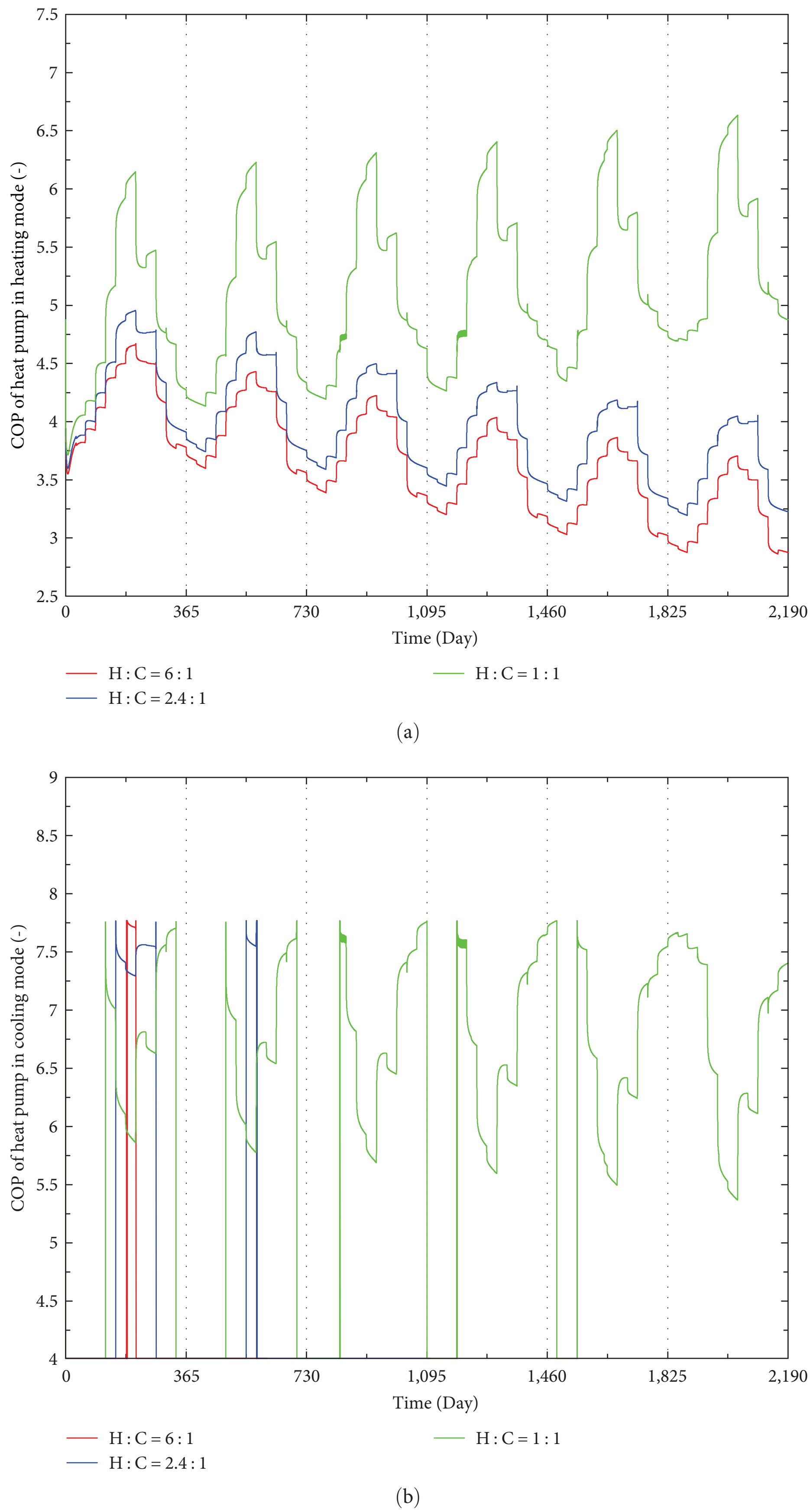

FIGURE 8: Variations in (a) COP of heat pump for heating load and (b) COP of heat pump for cooling load in the vertical GSHP system.

Table 3: Technical comparisons for GSHP heat pump systems coupled with two ground heat exchangers.

Ground heat exchanger	Horizontal ground loops	Vertical boreholes
Configurations	200 Single-layer U-tube pipes: (i) pipe length = 200.0 m (ii) burial depth = 3.0 m (iii) spacing of pipes = 1.0 m (iv) diameter of pipes = 0.04m (v) Land area = 80,000 m^2	200 vertical boreholes installed with single U-tube pipes: (i) borehole length = 210.0 m (ii) burial depth = 1.2 m (iii) spacing of boreholes = 8.0 m (iv) diameter of borehole = 0.14 m (v) diameter of pipes = 0.04 m (vi) Land area = 8,313.8 m^2
Soil profiles	Three layers: (i) 0–0.03 m topsoil (ii) 0.03–2.4 m silty clay (iii) 2.4–4.0 m mudstone	Three layers: (i) 0–1.2 m silty clay (ii) 1.2–158.8 m mudstone (iii) 158.8–210 m sandstone
Temperature boundaries	(i) Local climatic conditions on the ground surface (ii) A fixed temperature of 12.0°C at the depth of 4.0 m	(i) A fixed temperature of 10.62°C at the domain top (ii) A fixed temperature of 15.87°C at the domain owing to a temperature gradient of 25.0°C/1,000 m

heating-to-cooling ratios were 6 : 1 and 2.4 : 1 indicated a low-heat recovery potential of the system, while an upward trend in the fluid temperature when the heating-to-cooling ratio was decreased to 1 : 1 indicated a good heat storage ability of the system.

When considering the COPs of the heat pump as shown in Figures 6 and 8, although there are differences in the values of COPs, for both systems, reducing the heating-to-cooling ratio would increase the COP of the heat pump in heating mode but would decrease the COP of the heat pump in cooling mode. For example, in the horizontal system, during the heating mode, the lowest COP values were 3.62, 3.75, and 4.00 under heating-to-cooling ratios of 6 : 1, 2.4 : 1, and 1 : 1, respectively. That implies that when the heating-to-cooling ratio was decreased from 6 : 1 to 2.4 : 1 and 1 : 1, the lowest COP values in the heating mode were increased by approximately 3.6% and 10.5%, respectively. In contrast, the lowest COP values during the cooling mode were 7.54, 7.13, and 5.46 under heating-to-cooling ratios of 6 : 1, 2.4 : 1, and 1 : 1, respectively. Consequently, the lowest COP values in the cooling mode were reduced by 5.4% and 27.6%, respectively, as the heating-to-cooling ratio was decreased from 6 : 1 to 2.4 : 1 and 1 : 1. The simulated results revealed the significance of the heat injection process on the performance of GSHP systems.

Beyond the current study, it is worth comparing both systems from the economic and environmental perspective, and the life-cycle assessment will be the further research.

6. Conclusions

This study presents a quantitative investigation comparing the technical performance of GSHP systems coupled with horizontal ground loops and vertical boreholes, respectively, considering various heating-to-cooling ratios (6 : 1, 2.4 : 1, and 1 : 1). Through extensive simulations spanning multiple years, valuable insights into the system dynamics and efficiency have been obtained.

The simulated results reveal significant differences between the horizontal and vertical GSHP systems in terms of fluid temperatures and heat pump COPs. In the horizontal system, the fluid temperatures and COPs reached a steady annual cycle after 2 years, regardless of the heating-to-cooling ratios. However, in the vertical system, there was a general downward trend in the fluid temperatures for heating when the ratios were 6 : 1 or 2.4 : 1, while an overall upward trend was observed for a ratio of 1 : 1.

Quantitatively, the analysis demonstrates that the horizontal system exhibited a better heat recovery potential, with a COP range of 3.62–6.53 for heating under three heating-to-cooling ratios. In contrast, the vertical system displayed a superior heat storage ability, with increasing fluid temperatures and COPs for heating as the heating-to-cooling ratio decreased. Notably, the COPs for cooling mode in both systems were affected by the heating-to-cooling ratio, with higher ratios leading to longer cooling operational periods and lower COPs.

This study highlights the significance of design considerations and the impact of heating-to-cooling ratios on the performance of GSHP systems. The quantitative analysis provides valuable insights for the system optimisation and decision-making processes in the selection of horizontal or vertical configurations. Future research in this area can build upon these findings to further enhance the efficiency and sustainability of GSHP systems for heating and cooling applications.

Nomenclature

ρ: Density (kg/m^3)
θ: Volumetric content (-)
t: Time (s)
$\mathbf{v}$: Velocity (m/s)
u: Pressure (Pa)
γ: Unit weight (N/m^3)
K: Hydraulic conductivity (m/s)
y: Elevation (m)
h: Pressure head (m)
h_d: Scale parameter (m)
n: Shape parameter (-)
η: Shape parameter (-)

ν_v: Mass flow factor (-)
τ_v: Tortuosity factor (-)
φ: Porosity (-)
C_p: Specific heat capacity (J/kg/K)
S: Saturation (-) or pipe spacing (m)
T: Temperature (K)
L: Latent heat of vaporisation, 2.265×10^6 (J/kg) or pipe length (m)
λ: Thermal conductivity (W/m/K)
χ: Volume fraction (-)
H: Burial depth of pipes (m)
F: Heat flux (W/m^2)
r: Flow rate (m^3/s)
R: Outer radius of pipes (m)
b: Thickness of pipes (m)
D: Ground depth (m)
E: Evaporation flux (kg/m^2/s)
P: Rainfall (kg/m^2/s)
Q: Thermal load (W) or heat flow rate (W)
COP: Coefficient of performance (-).

Subscript or Superscript

j: Notation
i: Inlet
o: Outlet
s: Solid or saturated state
w: Water
a: Air
g: Ground
v: Vapour
l: Liquid water
f: Fluid in pipes
p: Pipes
NE: Net energy
NM: Net moisture
SW: Shortwave radiation
LW: Longwave radiation
SEN: Sensible heat radiation
LE: Latent heat radiation
AE: Actual evaporation
RO: Run-off
GHE: Ground heat exchanger.

Data Availability

All data are contained within the article.

Conflicts of Interest

The authors declare that they have no conflicts of interest.

Authors' Contributions

Wu Gao contributed in the writing—original draft and editing, methodology, software, and investigation. Shakil Masum contributed in the supervision and project administration. Liangliang Jiang and Shakil Masum contributed in the writing—review and editing. Wu Gao and Shakil Masum contributed in the conceptualisation.

Acknowledgments

This work was supported by EPSRC the funded "Integrated Heating and Cooling Networks with Heat-sharing-enabled Smart Prosumers" project (Grant number EP/T022795/1). The financial support for the authors is gratefully acknowledged.

References

[1] Intergovernmental Panel on Climate Change (IPCC), Working Group I Contribution to the IPCC Fifth Assessment Report (AR5), *Climate Change 2013: The Physical Science Basis*, IPCC, Stockholm, 2013.
[2] National Statistics, *Department for business, energy and industrial strategy (BEIS), 2021 UK greenhouse gas emissions, provisional figures*, 2022, https://assets.publishing.service.gov.uk/government/uploads/system/uploads/attachment_data/file/1064923/2021-provisional-emissions-statistics-report.pdf.
[3] D. Bertermann, H. Klug, L. Morper-Busch, and C. Bialas, "Modelling vSGPs (very shallow geothermal potentials) in selected CSAs (case study areas)," *Energy*, vol. 71, pp. 226–244, 2014.
[4] A. Casasso and R. Sethi, "G.POT: a quantitative method for the assessment and mapping of the shallow geothermal potential," *Energy*, vol. 106, pp. 765–773, 2016.
[5] S. Ikeda, W. Choi, and R. Ooka, "Optimization method for multiple heat source operation including ground source heat pump considering dynamic variation in ground temperature," *Applied Energy*, vol. 193, pp. 466–478, 2017.
[6] K. Bryś, T. Bryś, M. A. Sayegh, and H. Ojrzyńska, "Subsurface shallow depth soil layers thermal potential for ground heat pumps in Poland," *Energy and Buildings*, vol. 165, pp. 64–75, 2018.
[7] A. Dahash, F. Ochs, M. B. Janetti, and W. Streicher, "Advances in seasonal thermal energy storage for solar district heating applications: a critical review on large-scale hot-water tank and pit thermal energy storage systems," *Applied Energy*, vol. 239, pp. 296–315, 2019.
[8] C. S. A. Chong, G. Gan, A. Verhoef, R. G. Garcia, and P. L. Vidale, "Simulation of thermal performance of horizontal slinky-loop heat exchangers for ground source heat pumps," *Applied Energy*, vol. 104, pp. 603–610, 2013.
[9] S. E. Sofyan, E. Hu, and A. Kotousov, "A new approach to modelling of a horizontal geo-heat exchanger with an internal source term," *Applied Energy*, vol. 164, pp. 963–971, 2016.
[10] C. Li, J. Mao, H. Zhang, Z. Xing, Y. Li, and J. Zhou, "Numerical simulation of horizontal spiral-coil ground source heat pump system: sensitivity analysis and operation characteristics," *Applied Thermal Engineering*, vol. 110, pp. 424–435, 2017.
[11] E. Pulat, S. Coskun, K. Unlu, and N. Yamankaradeniz, "Experimental study of horizontal ground source heat pump performance for mild climate in Turkey," *Energy*, vol. 34, no. 9, pp. 1284–1295, 2009.
[12] A. Casasso and R. Sethi, "Efficiency of closed loop geothermal heat pumps: a sensitivity analysis," *Renewable Energy*, vol. 62, pp. 737–746, 2014.
[13] M.-J. Kim, S.-R. Lee, S. Yoon, and J.-S. Jeon, "An applicable design method for horizontal spiral-coil-type ground heat exchangers," *Geothermics*, vol. 72, pp. 338–347, 2018.

[14] A. Sedaghat, M. Habibi, and A. Hakkaki-Fard, "A novel ground thermal recovery system for horizontal ground heat exchangers in a hot climate," *Energy Conversion and Management*, vol. 224, Article ID 113350, 2020.

[15] Y. Gao, R. Fan, H. S. Li et al., "Thermal performance improvement of a horizontal ground-coupled heat exchanger by rainwater harvest," *Energy and Buildings*, vol. 110, pp. 302–313, 2016.

[16] N. Kayaci and H. Demir, "Long time performance analysis of ground source heat pump for space heating and cooling applications based on thermo-economic optimization criteria," *Energy and Buildings*, vol. 163, pp. 121–139, 2018.

[17] P. Hein, O. Kolditz, U.-J. Görke, A. Bucher, and H. Shao, "A numerical study on the sustainability and efficiency of borehole heat exchanger coupled ground source heat pump systems," *Applied Thermal Engineering*, vol. 100, pp. 421–433, 2016.

[18] C. Li, P. J. Cleall, J. Mao, and J. J. Muñoz-Criollo, "Numerical simulation of ground source heat pump systems considering unsaturated soil properties and groundwater flow," *Applied Thermal Engineering*, vol. 139, pp. 307–316, 2018.

[19] M. Soltani, P. Farzanehkhameneh, F. M. Kashkooli, A. Al-Haq, and J. Nathwani, "Optimization and energy assessment of geothermal heat exchangers for different circulating fluids," *Energy Conversion and Management*, vol. 228, Article ID 113733, 2021.

[20] H. Boughanmi, M. Lazaar, S. Bouadila, and A. Farhat, "Thermal performance of a conic basket heat exchanger coupled to a geothermal heat pump for greenhouse cooling under Tunisian climate," *Energy and Buildings*, vol. 104, pp. 87–96, 2015.

[21] H. Benli, "A performance comparison between a horizontal source and a vertical source heat pump systems for a greenhouse heating in the mild climate Elaziğ, Turkey," *Applied Thermal Engineering*, vol. 50, no. 1, pp. 197–206, 2013.

[22] J.-U. Lee, T. Kim, and S.-B. Leigh, "Applications of building-integrated coil-type ground-coupled heat exchangers—comparison of performances of vertical and horizontal installations," *Energy and Buildings*, vol. 93, pp. 99–109, 2015.

[23] P. Yin, M. Pate, and F. Battaglia, "In-field performance evaluation and economic analysis of residential ground source heat pumps in heating operation," *Journal of Building Engineering*, vol. 26, Article ID 100932, 2019.

[24] L. Aresti, P. Christodoulides, and G. A. Florides, "An investigation on the environmental impact of various ground heat exchangers configurations," *Renewable Energy*, vol. 171, pp. 592–605, 2021.

[25] W. Gao, S. Masum, J. Black, and H. R. Thomas, "Improving computational efficiency of numerical modelling of horizontal ground source heat pump systems for accommodating complex and realistic atmospheric processes," *Geothermics*, vol. 106, Article ID 102568, 2022.

[26] J. R. Philip and D. A. De Vries, "Moisture movement in porous materials under temperature gradients," *Eos, Transactions American Geophysical Union*, vol. 38, no. 2, pp. 222–232, 1957.

[27] R. H. Brooks and A. T. Corey, *Hydraulic Properties of Porous Media*, Colorado State University, Fort Collins, USA, 1964.

[28] M. T. van Genuchten, "A closed-form equation for predicting the hydraulic conductivity of unsaturated soils," *Soil Science Society of America Journal*, vol. 44, no. 5, pp. 892–898, 1980.

[29] H. R. Thomas and S. W. Rees, "Measured and simulated heat transfer to foundation soils," *Géotechnique*, vol. 59, no. 4, pp. 365–375, 2009.

[30] W. Gao, S. Masum, M. Qadrdan, and H. R. Thomas, "Estimation and prediction of shallow ground source heat resources subjected to complex soil and atmospheric boundary conditions," *Renewable Energy*, vol. 197, pp. 978–994, 2022.

[31] J.-M. Zhang, D. Tran, M. D. Fredlund, and D. G. Fredlund, "Coupling heat and moisture flow for the computation of actual evaporation," in *Proceedings of the Canadian Geotechnical Conference and Fifth Pan-American Conference*, pp. 2–6, Toronto, Canada, 2011.

[32] I. Staffell, D. Brett, N. Brandon, and A. Hawkes, "A review of domestic heat pumps," *Energy & Environmental Science*, vol. 5, no. 11, pp. 9291–9306, 2012.

[33] H. Qian and Y. Wang, "Modeling the interactions between the performance of ground source heat pumps and soil temperature variations," *Energy for Sustainable Development*, vol. 23, pp. 115–121, 2014.

[34] H. R. Thomas and Y. He, "Analysis of coupled heat, moisture and air transfer in a deformable unsaturated soil," *Géotechnique*, vol. 45, no. 4, pp. 677–689, 1995.

[35] O. C. Zienkiewicz, R.L. Taylor, and J. Z. Zhu, *The Finite Element Method: Its Basis and Fundamentals*, Elsevier, 6th edition edition, 2005.

[36] J. Douglas Jr. and B. F. Jones Jr., "On predictor–corrector methods for nonlinear parabolic differential equations," *Journal of the Society for Industrial and Applied Mathematics*, vol. 11, no. 1, pp. 195–204, 1963.

[37] J.-C. Calvet, P. Bessemoulin, J. Noilhan et al., "MUREX: a land-surface field experiment to study the annual cycle of the energy and water budgets," *Annales Geophysicae*, vol. 17, no. 6, pp. 838–854, 1999.

[38] G.-S. Enrique, I. Braud, T. Jean-Louis, V. Michel, B. Pierre, and C. Jean-Christophe, "Modelling heat and water exchanges of fallow land covered with plant-residue mulch," *Agricultural and Forest Meteorology*, vol. 97, no. 3, pp. 151–169, 1999.

[39] J. Hu, "An improved analytical model for vertical borehole ground heat exchanger with multiple-layer substrates and groundwater flow," *Applied Energy*, vol. 202, pp. 537–549, 2017.

[40] W. Li, X. Li, R. Du, Y. Wang, and J. Tu, "Experimental investigations of the heat load effect on heat transfer of ground heat exchangers in a layered subsurface," *Geothermics*, vol. 77, pp. 75–82, 2019.

[41] W. Gao, S. Masum, M. Qadrdan, and H. R. Thomas, "A numerical study on performance efficiency of a low-temperature horizontal ground-source heat pump system," *Energy and Buildings*, vol. 291, Article ID 113137, 2023.

[42] British Geological Survey (BGS), 2021, https://mapapps2.bgs.ac.uk/geoindex/home.html.

[43] J. Busby, "UK shallow ground temperatures for ground coupled heat exchangers," *Quarterly Journal of Engineering Geology and Hydrogeology*, vol. 48, no. 3-4, pp. 248–260, 2015.

[44] J. Busby, A. Kingdon, and J. Williams, "The measured shallow temperature field in Britain," *Quarterly Journal of Engineering Geology and Hydrogeology*, vol. 44, no. 3, pp. 373–387, 2011.

[45] F. Leij, W. Alves, M. van Genuchten, and J. Williams, *The UNSODA Unsaturated Soil Hydraulic Database: User's Manual*, National Risk Management Research Laboratory, Office of Research and Development, US Environmental Protection Agency, 1996.